River Flow 2010 - Dittrich, Koll, Aberle & Geisenhainer (eds) - © 2010 Bundesanstalt für Wasserbau ISBN 978-3-939230-00-7

Space-time correlation and momentum exchanges in compound open-channel flow by simultaneous measurements of two-sets of ADVs

M. Sanjou, I. Nezu & K. Itai
Department of Civil Engineering, Kyoto University, Katsura Campus, 615-8540, Kyoto, Japan

ABSTRACT: Compound open-channel flows are often observed in rivers in flood. These complex flows are highlighted in fundamental hydraulics as well as river engineering because they have various functions such as preventing water disaster, valuable open-spaces for aquatic lives and ecosystems. Recently, several highly-accurate turbulence measurements have been conducted with a two-component laser Doppler anemometer (LDA) and PIV, and they offer very valuable database of observed turbulent structures. However, all three components of large-scale flume data are not available as yet, because most of turbulence measurements of LDA and PIV were limited for miniature size flumes, in which the flume width was smaller than about 60cm. So, in the present study, 3D turbulence measurements with recently available acoustic Doppler velocimetry (ADV) were conducted in a 150cm wide large-scale compound channel flume. Furthermore, in this study, simultaneous measurements of two sets of ADV probes were also carried out in order to reveal space correlation properties of velocity fluctuations between the main-channel and the floodplain.

Keywords: Compound open-channel flows, Turbulence structure, Space correlation and simultaneous measurements by two sets of ADVs

1 INTRODUCTION

Compound open-channel flow is one of two-stage flows, that is to say, it is composed of main-channel and floodplains. Particularly, such complex flows are often observed in natural rivers in flood. Ikeda & McEwan (2009) have reviewed previous studies on the significant properties and sedimentation in compound open-channel flows. Many studies pointed out that coherent horizontal vortices appear with a constant spacing in the streamwise direction. These are generated by a shear instability associated with the velocity differences between the main-channel and floodplains in the similar mechanism to coherent vortices in mixing layers. Recently, several highly accurate turbulence measurements have been conducted with laser Doppler anemometer (LDA) and PIV, and they offer very valuable database of observed turbulent structures and coherent vortices. These vortices enhance mass and momentum exchanges significantly between the high-speed main-channel flow and the low-speed floodplain flow. Thus, such compound open-channel flows have been studied intensively in river environment and hydraulic engineering. Shiono & Knight (1991) proposed a depth-averaged analytical solution including the effects of secondary currents, and evaluated the lateral profiles of the apparent shear stress in large-scale compound flume. A possibility of measuring turbulent structures in compound open-channel flows has been opened up relatively recently with the development of non-intrusive measurement devices such as laser Doppler anemometer (LDA) and particle image velocimetry (PIV). Tominaga & Nezu (1991) have conducted accurate turbulence measurements in compound open-channel flows with a two-component LDA, and they revealed the cross-sectional distributions of primary velocity and secondary currents and proposed a generation mechanism of the apparent shear stress. The flow-visualization measurements such as PIV enable us to reveal horizontal vortex associated with shear instability near the junction region. The horizontal vortex was first identified by Sellin (1964), who conducted classical type flow visualization using powdered aluminum. New digital PIV techniques can evaluate the generation and transport mechanism, along with their periodicity and scale length. Nezu et al. (1999) revealed that a twin-vortex structure, which consists of counter-rotating vortex pairs, appears as

Table 1 Hydraulic condition

Q (l/s)	U_m (cm/s)	H (cm)	D (cm)	H/D	B_m (cm)	B (cm)	Re	*instrument*
63.0	15	40	20	2	60	150	60000	ADV (present)
8.4	35	8	4	2	20	40	28000	LDA(Tominaga&Nezu)

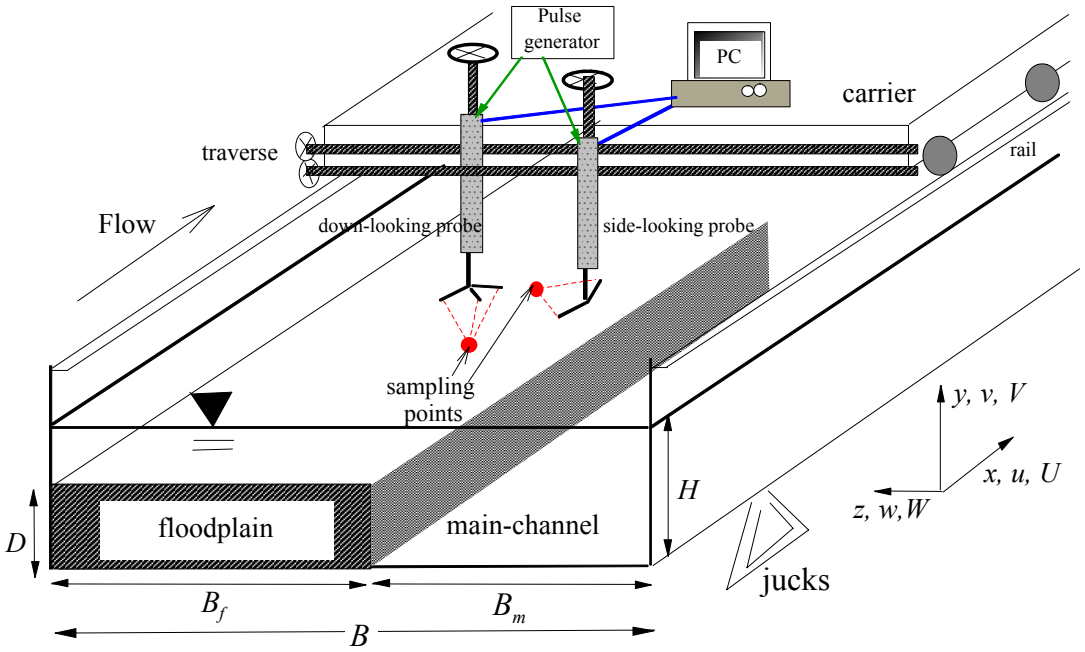

Figure 1. Experimental setup

water depth reaches 1.5 times the height of the floodplain. Nezu et al. (2004) further developed a dual-layer PIV system, in which different elevations of laser light sheet (LLS) were generated using a combination of three plane mirrors, and they revealed the convection properties in depth-varying unsteady compound channel flow. Meandering compound open-channel flow is also a one of high interesting topics in river engineering and flood mitigation. There are complicated distributions of mean velocity and turbulence components in these flows. In particular, significant cross-sectional secondary currents and horizontal vortices are generated due to an interaction between meandering in-bank main-channel flow and straight overbank floodplain flow. Recently Sanjou & Nezu (2009) conducted 3D PIV analysis to reveal instantaneous flow structures on horizontal planes located at different elevations simultaneously. In particular, they examined an interaction between turbulence structure in meandering compound open-channel flows.

However, all three components of velocity are not available as yet in large-scale open-channel flows, because most with turbulence measurements of LDA and PIV were limited for miniature size flumes, in which the flume width was about smaller than 60cm. These measured data are also needed to examine the calculation accuracy of above-mentioned computational simulations. So, in the present study, 3D turbulence measurements with recently available acoustic Doppler velocimetry (ADV) were conducted in a 150cm wide middle-scale compound channel flume which has just been constructed in our new Hydraulics Laboratory. Furthermore, in this study, simultaneous measurements of two sets of ADV probes were also conducted in order to reveal space correlation properties of velocity fluctuations between the main-channel and the floodplain.

2 EXPERIMENTAL PROCEDURE

2.1 *Experimental setup*

Figure 1 shows the present measurement setup and coordinate system, in which a 150cm wide middle-scale compound channel flume was used. The flume length is 10m and bed slope is 1/10000. The 20cm height acrylic boxes were set on the left-hand-side of the channel flume as a floodplain. B is the channel width, B_f is the floodplain width, B_m is the main-channel width, H is the water depth, and D is the height of the floodplain. x is the streamwise, y is the vertical and z is the spanwise coordinates. The origins of coordinates are x=0 at the channel entrance, y=0 at the flume bed and z=0 at the junction, respectively. The time-averaged velocity components in each direction are defined as U, V, W and the turbulence components are defined as u, v, w, respectively. Turbulence measurements were conducted by ADV (Sontek, micro ADV) and PIV. The ADV probe was traversed in the spanwise and vertical directions to obtain the cross-sectional distributions of mean velocity and turbulence components. Time-series of all three components of velocity were recorded simultaneously

(a) down-looking 3D probe

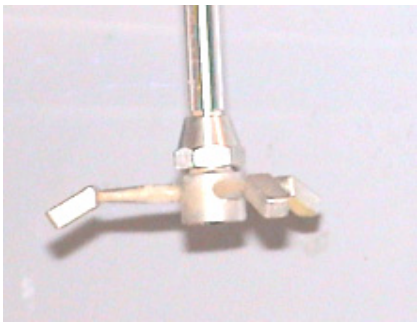

(b) side-looking 2D probe

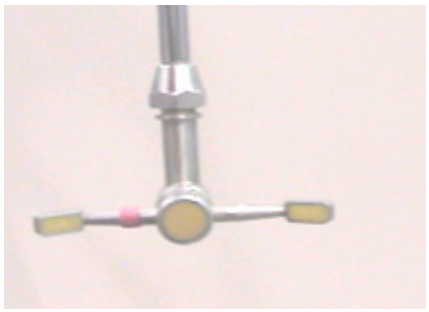

Figure 2. ADV probes of micro ADV (Sontek made) (a) down-looking 3D type and (b) side-looking 2D type

using 3D down-looking ADV probe (Figure 2a) which was traversed more than 5cm away from the free-surface. 2D side-looking ADV probe (Figure 2b) was also used for the compensating measurements near the free-surface. The noise and spike signals were removed by the wavelet method. As an advanced application, simultaneous measurements between the down-looking probe and the side-looking probe were conducted to reveal space correlation properties. A trigger signal from a pulse generator realizes simultaneous controls of two ADVs. The sampling rate was chosen as 50 Hz and sampling time of one point measurement is 60 sec.

2.2 *Hydraulic condition*

The hydraulic condition is shown in Table 1, in which LDA measurements conducted by Tominaga & Nezu (1991) were also included for comparison. The measuring section for ADV was 6m downstream from the channel entrance. In this study, the water depth was H=40cm, that is to say, the relative water depth $H/D=2.0$, which is the same value as LDA measurements. Of course, this relative water depth is much larger and also the aspect ratio is very low compared with the actual rivers. The discharge Q was 63.0 l/s. The bulk-mean velocity, U_m, was 15cm/s and the Reynolds number, $Re \equiv U_m H/\nu$, was 6.0×10^4 in the present measurements. In this study, as a first step to study turbulence structure in the middle-size compound flume, we chosen the present hydraulic condition which has same geometry as the accurate previous LDA data base. The present results will be useful for benchmark tests of the numerical simulations. In near future, another depth cases will be measured.

3 RESULTS AND DISCUSSIONS

3.1 *Cross-sectional distribution of streamwise velocity*

Figure 3 shows the distribution of time-averaged streamwise velocity U measured by ADV, which is normalized by maximum velocity $U_{\max}$. There are significant differences in streamwise velocity between the main-channel and floodplain. Consequently, the spanwise gradient of mean velocity $\partial U/\partial z$ is formed significantly near the junction, and thus it is suggested that horizontal vortices may be generated periodically due to the inflection point, e.g., see Nezu et al.(1999). In the junction zone between the main-channel and floodplain, one can see a bulge feature of streamwise velocity from junction edge toward the main-channel fee-surface. Such a bulge property is peculiar to secondary currents, as pointed out by many previous studies.

3.2 *Secondary currents*

Figure 4 shows the time-averaged secondary currents (V,W). The time-averaged vertical velocity components within the 5cm region from the free-surface could not be measured, because the down-looking probe cannot be operated in this region. So, the value of V was evaluated from the following continuity equation by using the measured data of U and W near the free-surface.

$$V=\int_y^H\left(\frac{\partial U}{\partial x}+\frac{\partial W}{\partial z}\right)dy \qquad (1)$$

In the centerline $(z/B_m=-0.5)$ of the main-channel, downflows are observed, and it causes the velocity dip, i.e., the maximum position of streamwise velocity appeared below the free-surface, which is marked as "x" in Figure 3. Of particular significance is that a large-scale clockwise and counter-clockwise circulations appear in the floodplain and the main-channel, respectively. These secondary currents form in the same fashion as observed in rectangular open-channel flows. The maximum magnitude of secondary currents, $(V^2+W^2)^{1/2}$, attains up to 4 % of $U_{\max}$, which is in good agreement with LDA data for smaller-scale flume

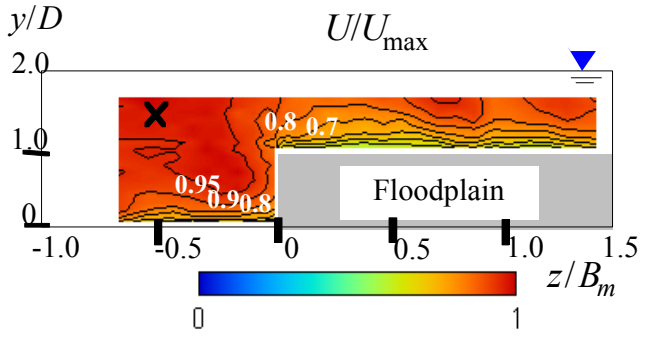

Figure 3. Distribution of streamwise velocity component ("x" indicates the maximum velocity position)

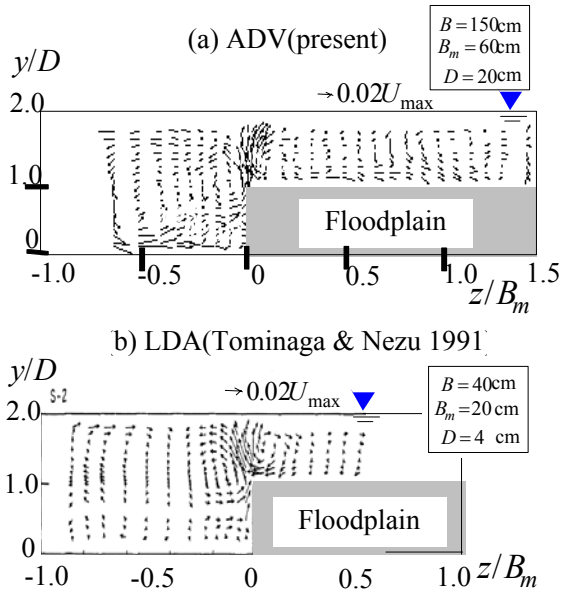

Figure 4. Distributions of secondary-currents velocity vectors, (a) present ADV and (b) LDA measurements by Tominaga & Nezu (1991)

3.3 *Distribution of bed shear stress*

It is very important to reveal the properties of bed-shear stress related to sediment transport and bed formation. Several methods are proposed for evaluating the friction velocity. In this study, the log-law was applied, and the present results were compared with those of Tominaga & Nezu (1991). Figure 5 shows the streamwise velocity profiles normalized by the inner variables at four different positions, i.e., (i) centerline of main-channel, (ii) main-channel region near the junction, (iii) floodplain region near the junction and (iv) centerline of floodplain, in which, dashed line is the log-law distribution given by

$$U^+ = 1/\kappa \cdot \ln y^+ + A \qquad (2)$$

in which, $U^+ \equiv U/U_*$, $y^+ \equiv yU_*/\nu$, $\kappa = 0.412$ and $A = 5.29$. Except for the floodplain centerline, the streamwise velocity decreases near the free-surface compared with the log-law. This may be because secondary currents influence the streamwise velocity significantly. Of particular significance is that the velocity profiles at all positions agree well with the log-law in

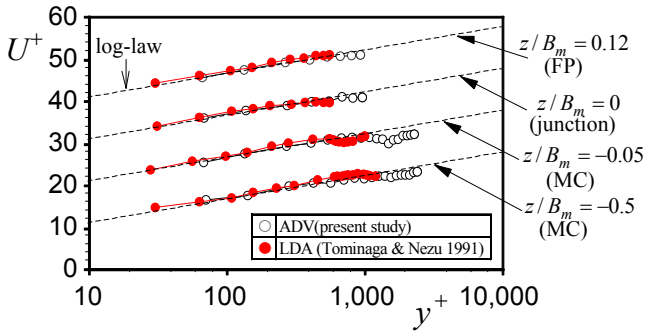

Figure 5. Sreamwise velocity profiles normalized by inner variables

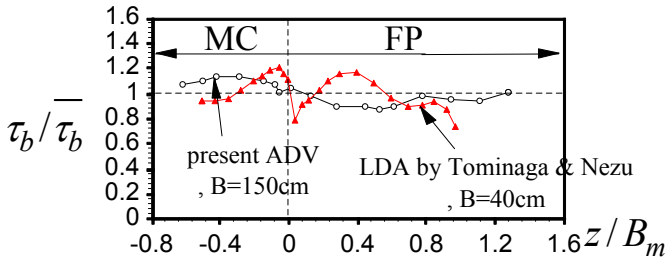

Figure 6. Spanwise distributions of bed-shear stress

the near–wall layer, i.e., $y^+ < 300$. It is noted that the log-law used in flat open-channels could be applied to even the junction region between the main-channel and floodplain, and the same properties were observed in both of the present ADV and LDA. These findings imply that the log-law method can be applicable in evaluation of friction velocity of compound open-channel flows.

Figure 6 shows the spanwise distributions of bed-shear stress, $\tau_b \equiv \rho U_*^2$, in which LDA data were also indicated for comparison. These results are normalized by the spanwisely-averaged value, $\overline{\tau_b}$. In the result of LDA, the positive peak is observed in the main-channel very near the junction. Local decrease appears in the junction region. This is because the streamwise velocity is comparatively small in this region. In the floodplain near the junction, the downflows transport the high-speed fluid toward the floodplain bed. The velocity gradient $\partial U/\partial y$ becomes large in this region as shown in Figure 3, and thus, the related bed-shear stress increases. Consequently, such two peaks of bed-shear stress appear in the main-channel and floodplain regions, respectively. Same feature is seen in both of the ADV and LDA data.

However, there are significant differences between the results of the ADV (middle-size flume) and LDA (small-size flume). The local decrease in the junction is much larger in the ADV than in the LDA. But this reason is unclear. Further, the peak positions are closer to the junction in the LDA results. This may be sidewall effect of the small-channel.

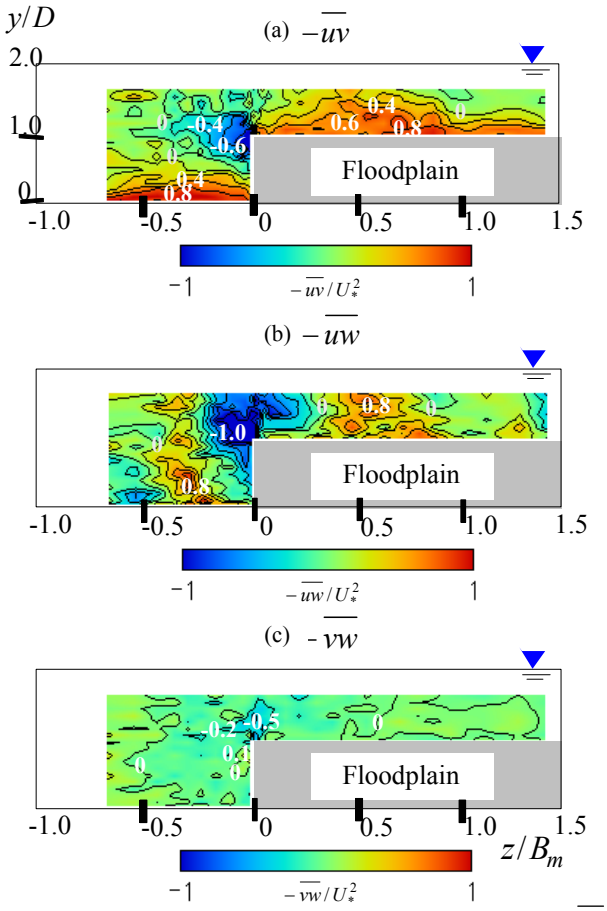

Figure 7. Distribution of all Reynolds stresses, (a) $-\overline{uv}$, (b) $-\overline{uw}$ and (c) $-\overline{vw}$

3.4 *Cross-sectional properties of Reynolds stress*

Figure 7 shows the distributions of all three components of Reynolds shear stress. Figures 7 (a), (b) and (c) correspond to $-\overline{uv}$, $-\overline{uw}$ and $-\overline{vw}$, respectively. These values are normalized by the friction velocity U_*. It should be noticed that $-\overline{uv}$ becomes positive near the main-channel bed and it decreases in the vertical direction. This tendency is similar to that observed in rectangular open-channel flows. This suggests that momentum transfer is promoted in the vertical direction near the bed. In contrast, negative values are observed near the free-surface. This is because the velocity gradient *dU/dy* is negative due to the velocity dip phenomena as shown in Figure 3.

The spanwise Reynolds stress $-\overline{uw}$ means the momentum exchanges on the horizontal plane. In the sidewall regions of the floodplain, negative distribution is observed corresponding to the sign of the spanwise velocity gradient *dU/dz*. Of particular significance is that the negative zone is accentuated near the junction between the main-channel and floodplain, and it is inferred from this result that horizontal vortices may cause high production of Reynolds stress. Consequently, mass and momentum exchanges are enhanced between the high-speed main-channel and the low-speed floodplain flows.

The present ADV could measure even the secondary Reynolds stress $-\overline{vw}$, the measurements of which are quite difficult with LDA and ADV system. The value of $-\overline{vw}$ becomes negative near the junction region, and this seems to correspond to secondary currents as shown in Figure 4. The gradient of $-\overline{vw}$ appears in the vorticity equation associated with secondary currents. Therefore, in the future work, it is expected that more detailed analysis allow us to reveal the generation mechanism of secondary currents in compound open-channel flows.

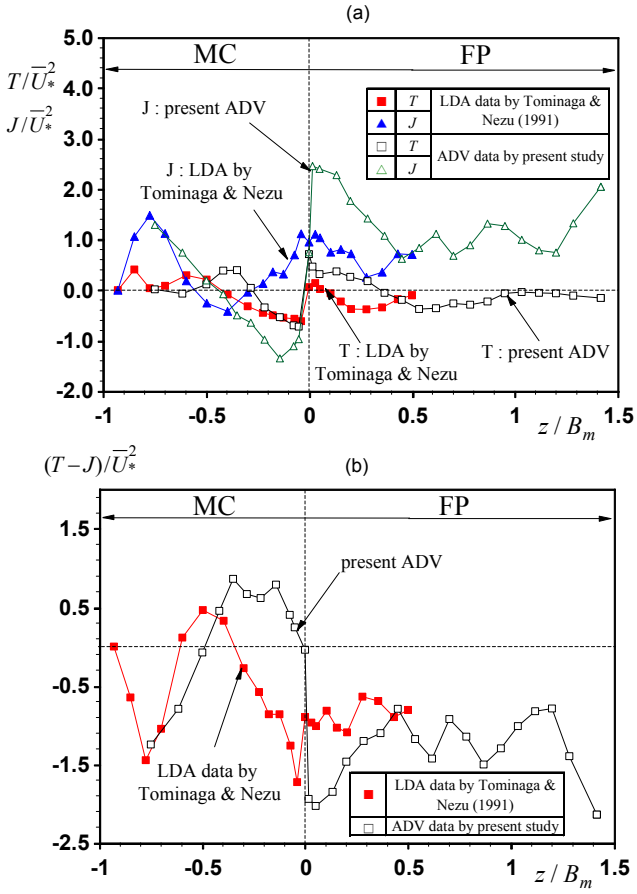

Figure 8. Distributions of contribution terms related to apparent shear stress

3.5 *Relation between secondary currents and bed-shear stress*

According to Nezu & Tominaga (1991), the depth-integration of streamwise momentum equation is reduced to the following equation.

$$\tau_b/\rho = gI_{ex}H' + \frac{d}{dz}H'(T-J) \qquad (3)$$

in which, H' is equal to be H in the main-channel, whereas, H' is to be $(H-D)$ over the floodplain. $\tau_b/\rho = (-\overline{uv} + \nu\partial U/\partial y)_{y=0}$ is the bed-shear

stress in the streamwise direction and I_e is the energy gradient.

$$T=\frac{1}{H}\int_{y_1}^{H'}-\overline{uw}dy \quad \text{and} \quad J=\frac{1}{H}\int_{y_1}^{H'}UWdy$$

are contribution terms to apparent shear stress generated by Reynolds stress $(-\overline{uw})$ and secondary currents (UW), respectively. y_1 =0 in the main-channel and $y_1=D$ in the floodplain.

Figure 8(a) shows the spanwise distributions of the apparent shear stress normalized by the spanwisely-averaged friction velocity $\overline{U}_*$. The secondary current term, J, has a positive peak near the junction, $z=0$, and decreases toward the main-channel and floodplain. These tendencies near the junction for the present ADV is very similar to those of LDA data. In contrast, the Reynolds stress term, T, has a negative peak, although there are some discrepancies. This seems to correspond to the generation of horizontal vortex induced by shear instability.

Figure 8(b) shows the distributions for the total of two kinds of contributions, $(T-J)$. The spanwise gradient of $(T-J)$ corresponds to an apparent shear stress. In the junction, negative peak appears in both results of ADV and LDA. This implies that a large apparent shear stress is produced significantly, and these features may be correlated with horizontal vortex formation. In near future, flow visualization such as PIV is needed to examine the effects of horizontal vortex on the shear stress near the junction between the main-channel and floodplain.

In compound open-channel flows, vertical momentum exchanges are also important, and the two-layer model proposed by Lin (1991) is examined in the followings. Depth-integration of momentum equation in the upper layer $(y>D)$ over the floodplain height, and one in the lower layer $(y<D)$ is reduced to the following two-kinds of shallow water, respectively.

(lower layer $y<D$)

$$\frac{\tau_b}{\rho}=gDI_e+\frac{d}{dz}\int_0^D-\overline{uw}dy-\frac{d}{dz}\int_0^D UWdy-UV_{y=D}+\frac{\tau_D}{\rho}$$

$$=gDI_e+\frac{d}{dz}DT_L-\frac{d}{dz}DJ_L-UV_{y=D}+\frac{\tau_D}{\rho} \qquad (4)$$

and

(upper layer $y>D$)

$$\frac{\tau_D}{\rho}=g(H-D)I_{ex}+\frac{d}{dz}\int_D^H-\overline{uw}dy-\frac{d}{dz}\int_D^H UWdy+UV_{y=D}$$

$$=g(H-D)I_{ex}+\frac{d}{dz}(H-D)T_U-\frac{d}{dz}(H-D)J_U+UV_{y=D} \quad (5),$$

in which $\tau_D/\rho=(-\overline{uv}+\nu\partial U/\partial y)_{y=D}$ means shear stress in the boundary plane between the upper and lower layers.

Figure 9 shows the distributions of contribution terms related to the apparent stress in Eqs. (4) and (5). The total value of the lower layer is negative in $z/B_m>-0.14$, and this suggests τ_b decreases near the junction between the main-channel and the floodplain. Around $z/B_m=-0.3$, the secondary-current contribution, J_L, becomes large. In contrast, at $z/B_m=-0.2$, $UV_{y=D}$ has a positive peak which means significant interactions between the upper and lower layers.

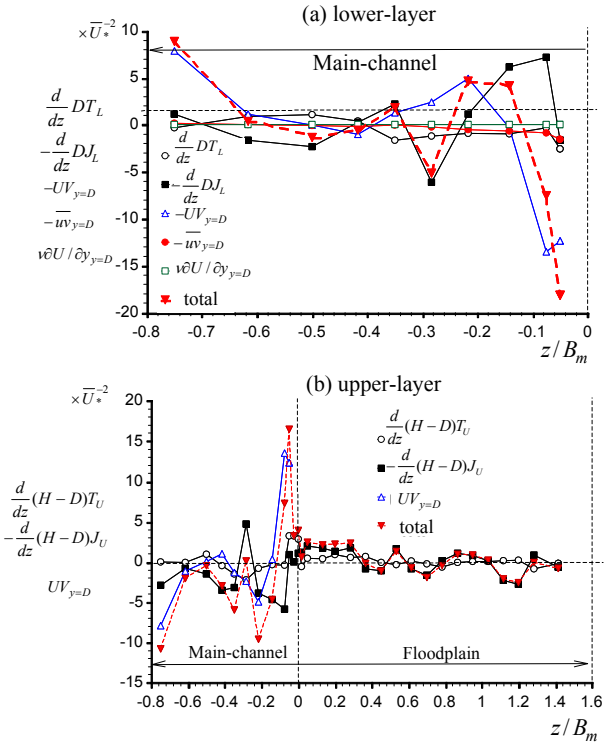

Figure 9. Distribution of apparent shear stress using two-layer model

The total value of the upper layer has positive and negative in the floodplain and main-channel near the junction. It is found that the contribution of J_U is twice to four times as large as that of T_U in the floodplain region, $0<z/B_m<0.3$. This suggests that secondary currents have more significant than the turbulence for generation of bed-shear stress. The total value in the main-channel region corresponds to the shear stress between the upper and lower layers, and it is found that $UV_{y=D}$ becomes large associated with upward flow from the junction edge toward the main-channel free-surface as shown in Figure 4. Of particular significance is that contributions of turbulence and secondary currents varies in the spanwise direction related to the distributions of Reynolds stress and time-averaged velocity components.

3.6 *Relation between secondary currents and bed-shear stress*

Secondary currents and turbulence influence the shear stress significantly. In this section, the correlation analysis was conducted to consider transport properties

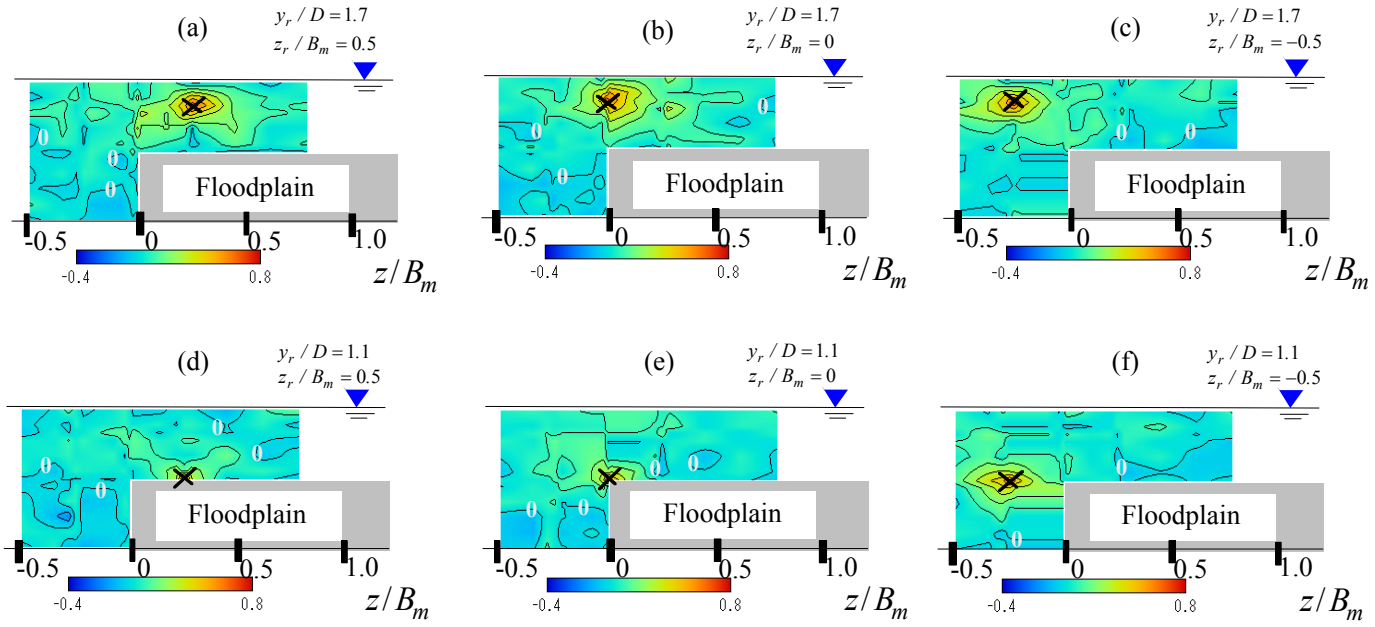

Figure 10. Cross-sectional distribution of correlation function, C_{ww} "x" indicates the reference position.

of turbulence and relation with secondary currents. Six reference points, (a) to (f), were given as shown in Figure 10, i.e., $(y/D, z/B_m) = (1.7,\ 0.5)$, (1.7, 0), (1.7, -0.5), (1.1, 0.5), (1.1, 0) and (1.1, -0.5). Figure 10 shows the distribution of space correlation function, C_{ww}, given by

$$C_{ww} = \frac{\overline{(w(y,z) - W(y,z)) \times (w(y_o,z_o) - W(y_o,z_o))}}{w'(y,z) \times w'(y_o,z_o)} \qquad (6)$$

in which, the over-bar means time-average operation.

It is found that (i)the spanwise diffusion is observed more significantly than the vertical one in Figure 10(d), (ii) a bulge feature is observed from the junction edge toward the free-surface of the main-channel in Figure 10(e) and (iii) a bulge appears below the reference point in Figure 11(f). It is inferred that these tendencies are induced by secondary currents as shown in Figure 3. In the results of (a), (b) and (c), C_{ww} distributes more largely in the spanwise direction than in the vertical one.

The ratio of spanwise length scale L_z to vertical one L_y is defined as

$$L_z / L_y \equiv \int_{z1}^{z2} C_{ww} dz \Big/ \int_{y1}^{y2} C_{ww} dy \qquad (7)$$

z_1 and z_2 are the spanwise terminal positions of the measured region. $y_1 = 0$ and $y_2 = 0.9H$. L_z / L_y at reference points (a), (b) and (c) were 1.60, 1.39 and 1.46, respectively. These results suggest that mean eddy scale is larger in the spanwise direction than in the vertical one. The value of (b) is the smallest because large upflow promotes more significantly generation of vertical mean eddy scale than that of spanwose mean eddy scale. It is revealed from the correlation analysis that mean eddy scales are influenced strongly by the secondary currents.

4 CONCLUSIONS

In the present study, ADV measurements in middle-scale compound open-channel flows. The ADV results allowed us to consider statistical properties of mean and turbulence components. The main results are as follows.

1)It is recognized that typical secondary currents are formed in near the junction in the same manner as observed in many previous studies. The distribution of streamwise velocity was influenced strongly by secondary currents and thus the velocity dip phenomena appear in the main-channel.

2)It is found that Reynolds stress is generated significantly associated with the gradient of streamwise velocity. In particular, the spanwise Reynolds stress $-\overline{uw}$ corresponds well to the generation of horizontal vortex.

3)Depth-integration analysis allows us to understand the relation between the secondary currents and turbulence and also the examine contribution properties of them to generation the apparent shear stress.

4)Two layer model is very useful to understand the relation between the upper and lower layers in the main-channel. Particularly, the spanwise features of their interaction were examined quantitatively .

5)Simultaneous measurements with two sets of ADV probes allow us to conduct correlation analysis of velocity fluctuations, It was revealed that velocity fluctuations are influenced strongly by secondary currents.

REFERENCES

Ikeda, S. and McEwan, I.K. 2009. Flow and sediment transport in compound channels, IAHR MONOPRAPH SERIES.

Lin, B. Y. 1991. Study on sediment transport and bed evolution in compound channels, Ph.D. Thesis, Kyoto University.

Nezu, I. and Nakagawa, H. 1993. Turbulence in open-channel flow, IAHR monograph, Balkema.

Nezu, I. Onitsuka, K., and Iketani K. 1999. Coherent horizontal vortices in compound open-channel flows, HYDRAULIC MODELING(ed. Singh et al.) Water Resources Pub., Colorado, 17-32.

Nezu, I. ,Sanjou, M. and Goto, K. 2004. Transition process of coherent vortices in depth-varying unsteady compound open-channel Flows, Shallow Flows(ed. G.H.Jirka& W.S.J. Uijttewaal), Balkema, 251-258.

Sanjou, M. and Nezu, I. 2009. Turbulence structure and coherent motion in vegetated open-channel flows, Journal of Hydraulic Research, 47, 598-610.

Sellin, R.H.J. 1964. A laboratory investigation into the flow in the channel of a river and that over floodplain, La Houille Blanche, 7, 22-26.

Shiono, K., Knight, D. W. 1991. Turbulent open-channel flow with variable depth across the channel, J. of Fluid Mech., 222, 617-646.

Tominaga, A. and Nezu, I. 1991. Turbulent structures in compound open-channel flow, J. of Hydraulic Eng.,117, 21-41.